Construction and Building Materials 446 (2024) 138015

Contents lists available at ScienceDirect

Construction and Building Materials

journal homepage: www.elsevier.com/locate/conbuildmat

Pozzolanic reactivity of carbonated high-calcium fly ash: A mechanism study

Gao Deng [a,b,c], Nannan Zhang [a,b,c,1], Wenyu Liao [c], Hongyan Ma [c,*], Yongjia He [a,b,**], Linnu Lu [d], Lingyu Chi [e]

[a] State Key Laboratory of Silicate Materials for Architectures (Wuhan University of Technology), Luoshi Road 122, Wuhan 430070, China
[b] School of Materials Science and Engineering, Wuhan University of Technology, Wuhan 430070, China
[c] Department of Civil, Architectural, and Environmental Engineering, Missouri University of Science and Technology, Rolla, MO 65401, USA
[d] Hubei Key Laboratory of Theory and Application of Advanced Materials Mechanics, School of Science, Wuhan University of Technology, Luoshi Road 122, Wuhan 430070, China
[e] Department of Chemistry, Missouri University of Science and Technology, Rolla, MO 65401, USA

ARTICLE INFO

Keywords:
High-calcium fly ash
Carbonation
Pozzolanic reactivity
Hydration products
Calorimetry

ABSTRACT

This research investigates the impact of accelerated carbonation treatment on the pozzolanic reactivity of high-calcium fly ash (HFA) by monitoring the reaction heat of HFA/carbonated HFA (CFA)-calcium hydroxide (CH) blends, and elucidates the underlying factors influencing the pozzolanic reactivity. The results indicate that in HFA/CFA-CH blends, CFA exhibits a comparable pozzolanic reactivity to that of HFA. This is attributed to the carbonation products accelerating the formation of monocarboaluminate (main) and C-S-H, compensating for the reduced heat resulting from the diminished highly reactive components after the carbonation treatment. Additionally, the increased surface area due to carbonation treatment is favorable for the pozzolanic reaction of CFA. However, in the HFA/CFA-CH blends with gypsum, the carbonation treatment adversely affects the pozzolanic reactivity of HFA since gypsum limits the monocarboaluminate formation. Overall, these findings suggest that when proportioned and used properly, CFA can retain comparable pozzolanic reactivity to that of the untreated HFA, while storing CO_2 permanently.

1. Introduction

Despite cement constituting less than 15 % of the total concrete mass, it contributes to over 85 % of concrete's carbon footprint [1]. Annually, the production of more than 4 gigatonnes (Gt) of cement leads to 7 % of the world's total anthropogenic CO_2 emissions [2–4]. To address the carbon footprint challenge within the cement industry, the utilization of industrial byproducts such as fly ash (FA) as supplementary cementitious materials (SCMs) has developed as a cost-effective approach to partially replace, and, thus, reduce the demand for traditional cement in concrete production [5,6].

FA is a finely powdered material derived from the residual inorganic matter produced during the combustion of pulverized coal in coal-fired power plants. Based on its calcium content, FA can be classified into low-calcium FA (LFA), typically containing less than 10 % calcium oxide (CaO), and high-calcium FA (HFA) [5]. LFA is commonly used in the construction industry as an SCM in concrete mixtures due to its capability to enhance workability, increase long-term strength, and improve durability [7]. Conversely, the application of HFA can be less preferred because it contains free-CaO, which could negatively affect the soundness and durability of concrete due to potential volume expansion [8].

In recent years, carbonation techniques have gained prominence as innovative methods for counteracting anthropogenic CO_2 emissions [9]. This technique involves utilizing disposal or waste materials to capture and sequester CO_2 [10–12]. The accelerated carbonation treatment of HFA has gained interest, as it not only rapidly sequesters CO_2 but also eliminates free-CaO, thereby ensuring its secure utilization in construction materials [8,13]. Siriruang et al. [8] and Pei et al. [14] studied

* Corresponding author.
** Corresponding author at: State Key Laboratory of Silicate Materials for Architectures (Wuhan University of Technology), Luoshi Road 122, Wuhan 430070, China.
E-mail addresses: mahon@mst.edu (H. Ma), hyj@whut.edu.cn (Y. He).
[1] This author contributed equally to the first author

https://doi.org/10.1016/j.conbuildmat.2024.138015
Received 21 May 2024; Received in revised form 18 August 2024; Accepted 19 August 2024
Available online 25 August 2024

Table 1
Chemical compositions of HFA.

Oxide	CaO	SiO_2	Al_2O_3	Fe_2O_3	MgO	SO_3	Na_2O	Mn_2O_3	K_2O	P_2O_5
HFA	26.16	38.82	19.52	6.22	3.65	1.07	1.22	0.44	0.77	0.90

the expansion of cement paste containing FA with and without carbonation treatment. Results showed that carbonation treatment of FA significantly improved the stability of cement pastes due to the reduction of free-CaO after the carbonation reaction. Chen et al. [15] applied carbonation curing and carbonated fly ash (CFA) to improve the performance of mortar samples and found that the freeze-thaw and sulfate attack resistance was improved. This improvement was associated with the consumption of free-CaO and calcium hydroxide (CH) during the carbonation curing. Additionally, they noted that the carbonation treatment of FA could increase the particle size and reduce the specific surface area due to the reaction products adhering to the surface [13], which was hypothesized to reduce the reactive contact area and affect the pozzolanic reactivity [16]. The pozzolanic reactivity of particular pozzolanic materials relies on chemistry or mineralogy mainly referring to active phases and physical characteristics such as specific surface area, particle size and surface morphology [17–19]. FA generally consists of three different components: a vitreous/amorphous phase (mainly), a certain amount of crystalline phases, and few unburned carbon [20,21]. The quantity of reactive crystalline phases has been suggested to determine the reactivity of FA [20]. And FA with a higher amorphous content is expected to enhance the pozzolanic reaction more effectively [21]. This reaction involves a chemical reaction between the active silica and alumina present in FA and CH to form calcium silicoaluminate hydrate, typically found in Portland cement-SCMs systems [22,23]. Carbonation treatment is expected to significantly affect the phases composition HFA, particularly the carbonation-active phases such as lime and calcium silicate/aluminate, and notably alters the surface properties of HFA, which inevitably influences the ion dissolution and reaction characteristics. This highlights the importance of studying the impact of carbonation treatment on the physical and chemical properties as well as the pozzolanic reactivity of HFA, which, however, has been barely studied.

Furthermore, the carbonation treatment of HFA alters the phase distribution of cement pastes substituted with partial CFA, particularly in the aluminate hydration products of CFA-blended cementitious materials. The presence of $CaCO_3$ in CFA resulting from carbonation treatment can react with aluminate phases to form monocarboaluminate (Mc) and hemicarboaluminate (Hc), resulting in the stabilization of ettringite [24–26]. This change in the phase assemblage may significantly affect the micro/macro mechanical properties and transport properties of concrete, impacting the durability and service life of cement-based materials [27,28]. Therefore, deeply understanding the characteristics and properties of CFA is essential for achieving the desired performance of CFA-incorporated carbon-efficient materials.

Various direct and indirect test methods have been developed to determine the pozzolanic reactivity of pozzolans. These methods include the strength activity index (SAI) test, the Chapelle test, the Frattini test, the saturated lime test, the isothermal calorimetry-based tests, and the 'rapid, reproducible, and reliable pozzolanic reactivity test' (R^3 test) [17,18,29–33]. The R^3 test can evaluate the pozzolanic reactivity of SCMs (e.g., calcined clay) by testing heat release using an isothermal calorimeter and analyzing the bound water of the SCMs in a specially designed chemical mixture. A modified R^3 test has also been developed to measure the heat evolution of SCMs-CH mixtures with 0.5 M potassium hydroxide at 50°C for 240 h through an isothermal calorimeter. This modified test allows the assessment of pozzolanic reactivity of SCMs by analyzing the heat release and CH consumption [32,33], which was supposed to better mimic the chemical environment in cement-based materials and evaluate the potential of pozzolanic reaction.

In this research, the modified R^3 method was adopted to assess the pozzolanic reactivity of CFA. The higher temperature of 50°C accelerates the pozzolanic reaction, enabling the prediction of the reaction degree in long-term pozzolanic reaction. At the same time, the CFA-CH mixture can be used to simulate the pozzolanic reaction of CFA in cement systems. This study is structured into two main sections. Firstly, the physical and chemical characteristics of HFA before and after carbonation treatment were investigated using XRD, TGA, FTIR, XPS, and ^{27}Al and ^{29}Si MAS NMR techniques. This section aimed to understand how CFA affects the pozzolanic reactivity of HFA. Building on the insights gained from the first section, the second part investigated the pozzolanic reactivity of CFA and its reaction products. Furthermore, 5 % gypsum was added to study the potential competing effects of carbonates and sulfates on aluminates, along with the impact of sulfate on pozzolanic reaction characteristics of CFA.

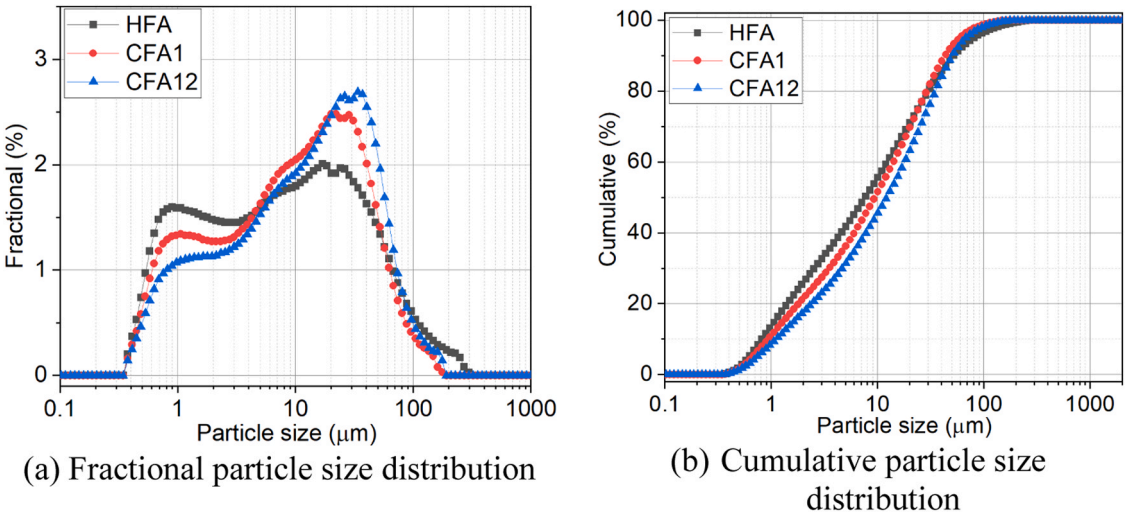

Fig. 1. Particle size distribution of HFA and CFA with different carbonation durations.

2. Experimental program

2.1. Raw materials and samples preparation

A high calcium fly ash (HFA) was used in this study, and its chemical composition was measured by X-ray fluorescence (XRF) as presented in Table 1. It is worth noting that the high CaO content (26.16 %) of the HFA is attributed to several different phases, such as hatrurite, ettringite, brownmillerite, and calcite, as will be discussed in Section 3.1.1. Free lime was not detected, perhaps because the free lime was carbonated during the storage in the air. Apart from the HFA, reagent-grade potassium hydroxide and calcium hydroxide were used in the pozzolanic reactivity test.

Carbonated FA (CFA) was prepared through a gas-solid accelerated carbonation treatment of HFA. In this process, HFA was thoroughly mixed with 15 % of deionized water (by mass of HFA) and evenly spread on a 45 μm sieve in a thin layer, around 2–3 mm, to ensure a homogeneous carbonation. The mixture was then exposed to pure CO_2 (99.9 %) at room temperature of 23±2°C and a pressure of 0.2 MPa. Carbonation durations of 1 h and 12 h were employed, and the corresponding CFA samples were labeled as CFA1 and CFA12, respectively. After the carbonation treatment, the samples were dried in a vacuum oven at 40°C for 24 h. Subsequently, they were ground using a Retsch RS200 vibratory disc mill for 6 s since FA particles were adhered together after carbonation treatment. The ground CFA was then sieved through a 75 μm mesh to achieve a particle size distribution as close as possible to that of HFA. The particle size distribution comparison in Fig. 1 indicates slight difference in the particle size distribution of HFA and CFA, mainly in the 0.6-to-4 μm and 10-to-40 μm particle sizes, attributed to the carbonation products formed on the surface of HFA particles, which will be elaborated on later.

The pozzolanic reactivity of HFA, CFA1 and CFA12 was investigated. As sulfates commonly exist in cement and can influence hydration products and accelerate the pozzolanic reaction, the impact of sulfate on the pozzolanic reaction of CFA was also studied by adding an additional 5 % gypsum (by mass of CH and FA). Pozzolanic reaction test was prepared by mixing a 3-to-1 mass ratio of CH and HFA/CFA in a 0.5 M potassium hydroxide solution with a liquid/solid ratio of 0.9, following established methodologies [32,33]. The potassium hydroxide solution was pre-prepared and maintained at around 20°C before use. Around 40 g of paste was mixed for 2 min using a handheld electric mixer. Subsequently, 15 g of paste was used for the heat release test using an 8-channel isothermal calorimeter (TAM Air, TA instruments), while the remaining pastes were sealed in tubes and cured for specific ages. These tests were performed at temperatures of 20°C and 50°C. The samples, with or without gypsum, cured at 50°C, were labeled as R0G, R1G, R12G, R0, R1, R12. Those cured at 20°C were labeled as 20R0, 20R1, and 20R12. Heat flow data were collected for 240 h, after which the samples were removed from the ampoule and their hydration was stopped using pure isopropanol for 7d and then dried in a vacuum oven at 40°C for 2d.

To investigate the ions evolution during the pozzolanic reaction of HFA and CFA, a slurry of HFA/CFA-CH was prepared. The mix proportion of the slurry was similar to that of the pozzolanic activity test, except that the liquid/solid ratio was adjusted from 0.9 to 5. 100 g of slurry was prepared for each mixture. These samples were then placed in HDPE bottles and agitated on a shaker at 200 rpm and at a temperature of 50°C for specified durations. At designated time points, a small portion of the suspension was collected using a syringe and filtered through a 0.22 μm filter in preparation for ion measurements.

2.2. Testing methods

The specific surface area of HFA and CFA was determined using a multi-station BET surface area analyzer (Nova 600 BET). Samples were fully dried in a vacuum oven at 40°C before the test. For each measurement, around 4 g of samples were added into the testing tube and then analyzed automatically following the SARM 2005 test program.

X-ray diffraction (XRD) patterns were collected using a Philips X-Pert diffractometer equipped with a Cu target operating at 45 kV and 40 mA. The scanning rate was set at 5°/min for general XRD patterns, while quantitative XRD (QXRD) patterns were scanned at a rate of 2°/min. For QXRD, the XRD-Rietveld refinement method was employed, utilizing 10 wt% α-Al_2O_3 powder as the internal standard.

The thermal gravimetric analysis (TGA) was conducted using a TA Instrument (SDT Q600). Samples were tested from 40°C to 1000°C at a heating rate of 10 °C/min under a N_2 atmosphere. Prior to the thermal test, powder samples were dried in a vacuum oven at 40°C for 24 h. According to previous works [34,35], the temperature ranges of 410–500°C and 500–850°C can be identified as the decomposition temperatures for CH and $CaCO_3$, respectively. And based on the thermal analysis results, the content of $CaCO_3$, degree of carbonation (DOC) and CO_2 uptake of samples were calculated according to Eqs. (1–4):

$$CO_2(\%) = \frac{\Delta m_{CO_2}}{M_{850^\circ C}} \times 100 \tag{1}$$

$$CO_{2uptake}(\%) = CO_{2carbonated}(\%) - CO_{2initial}(\%) \tag{2}$$

$$CaCO_3(\%) = CO_2(\%) \times \frac{100.09}{44.01} \tag{3}$$

$$\xi_{CaO}(\%) = \frac{CaCO_3(\%) \times \frac{56.08}{100.09}}{CaO_{RM}(\%)} \times 100 \tag{4}$$

where, Δm_{CO_2} is the mass loss due to $CaCO_3$ decomposition at 500–850°C; $M_{850^\circ C}$ is the mass of samples at a specific temperature; $CO_{2initial}$ and $CO_{2carbonated}$ are the weights of CO_2 derived from $CaCO_3$ in the samples before and after carbonation treatment, respectively; ξ_{CaO} is the DOC of samples; CaO_{RM} is the CaO content of the raw materials, which is obtained from the XRF analysis.

The ^{27}Al and ^{29}Si MAS NMR spectra were collected using a solid-state NMR spectrometer (AVANCE III 400 MHz WB, Bruker Co.). For the measurements, a 7 mm ZrO_2 rotor was utilized for both ^{27}Al and ^{29}Si NMR analysis, with a spinning speed set to 7.5 kHz. The spin relaxations were set at 2 s for ^{27}Al and 30 s for ^{29}Si NMR. Each sample ran for 1024 cycles, and subsequent adjustments of the spectra were performed using TopSpin 4.3.0 software.

Fourier transformation-infrared spectroscopy (FT-IR) was used to analyze the microstructure of carbonation products. The analysis was performed using a Nicolet iS50 FT-IR spectrometer, covering the spectral range of 4000–400 cm^{-1} and employing 32 scans for each measurement.

X-ray photoelectron spectroscopy (XPS) was conducted using a Kratos Axis 165 Photoelectron Spectrometer equipped with a monochromatic Al Kα X-ray source. The regional XPS scans were collected in 0.1 eV increments, and the retardation voltage was calibrated based on the positioning of the C1s peak.

Scanning electron microscopy (SEM) was conducted by a Helios Hydra CX in high vacuum mode, with an accelerating voltage of 10 kV, a beam current of 0.2 nA, and a working distance of approximately 4 mm. Before SEM/EDS tests, all samples were coated with a thin film of Au/Pt for 1 min to enhance conductivity.

An inductively coupled plasma-optical emission spectrometer (ICP-OES) with a liquid autosampler was used to determine the concentrations of elements. Prior to the test, the instrument was calibrated using standard solutions at different concentrations. The collected initial suspensions were filtrated through a 0.22 μm nylon filter and then diluted with 1 % nitric acid before analysis.

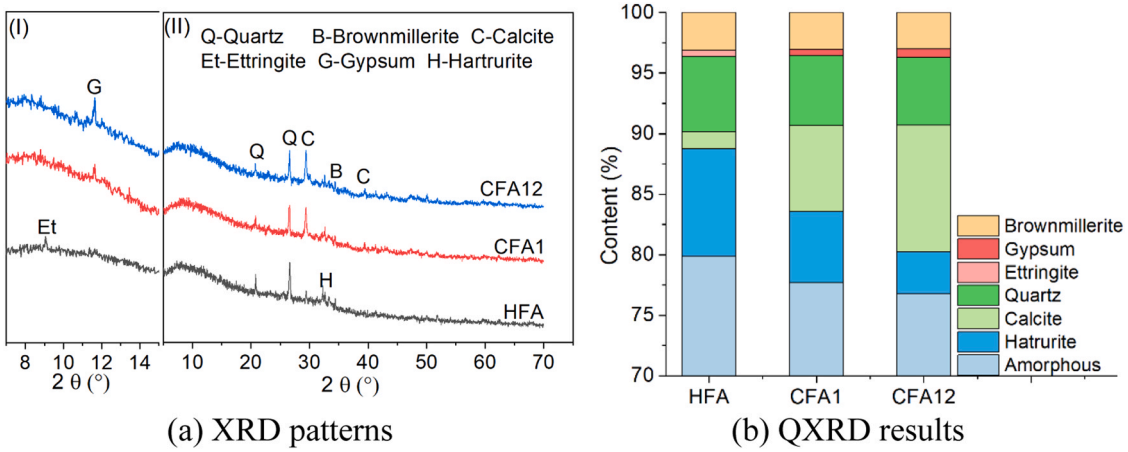

Fig. 2. XRD patterns and QXRD results HFA and CFA with different carbonation durations.

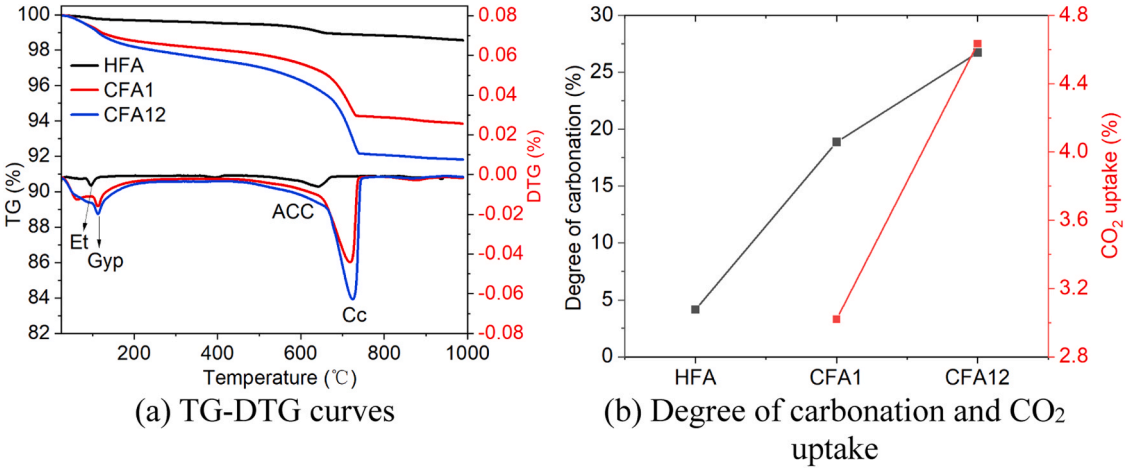

Fig. 3. Thermal analysis results, carbonation degree and CO_2 uptake of HFA and CFA with different carbonation durations.

3. Results

3.1. Carbonation treatment of HFA

3.1.1. Effect of carbonation on phase assemblage of HFA

The XRD patterns of the original HFA and CFA carbonated for 1 and 12 h are shown in Fig. 2(a), with the corresponding QXRD results shown in Fig. 2(b). In Fig. 2(a), the segment labeled as (I) represents a magnified view of the region labeled as (II). The original HFA consisted of around 80 % amorphous compounds and several dominant crystalline phases, including hatrurite, quartz, and brownmillerite. Traces of ettringite were also present in the original HFA. In addition, a small amount of pre-existing calcite was detected in HFA, likely resulting from the reaction of fresh HFA with CO_2 in the atmosphere during storage. Unlike in common high-calcium fly ashes, free lime was not detected in the used HFA, perhaps because of the natural carbonation in the air. The accelerated carbonation treatment enhanced the formation of calcite, with hatrurite primarily serving as a calcium source following Eqs. (5–8) [36,37] due to its reactivity to CO_2 [38]. A 1 h-carbonation treatment resulted in around 7 % calcite formation, and the content of calcite increased with increasing carbonation durations. Brownmillerite appeared to be inert under the CO_2 condition as its content remained stable after carbonation treatment. However, ettringite was no longer detected in the CFA samples as ettringite was not stable under the CO_2 condition due to the reaction of ettringite and CO_2 (Eq. (9)) [39], which resulted in the formation of gypsum. This observation was supported by the TG-DTG results in Fig. 3(a), in which the peak at around 100°C related to ettringite decomposition disappeared after carbonation treatment, and a new peak at around 120°C related to gypsum decomposition was formed. It should be noted in Fig. 3(a) that in addition to a sharp peak at around 720°C related to the decomposition of crystalline calcite, a slow mass loss between 450°C and 650°C was observed, which was likely attributed to the amorphous calcium carbonate (ACC) formation, as indicated by previous studies [40,41]. Fig. 3(b) shows the DOC and CO_2 uptake of CFA with different carbonation durations. A 1 h-carbonation treatment resulted in a 19 % DOC, and after 12 h of carbonation, the DOC increased to around 27 %, corresponding to a CO_2 uptake of around 4.6 %.

$$(CaO)_3{\cdot}SiO_2 + H_2O \rightarrow (CaO)_x{\cdot}SiO_2{\cdot}(H_2O)_y + Ca(OH)_2 \quad (5)$$

$$Ca(OH)_2 + CO_2 \rightarrow CaCO_3 + H_2O \quad (6)$$

$$(CaO)_3{\cdot}SiO_2 + CO_2 + H_2O \rightarrow (CaO)_x{\cdot}SiO_2{\cdot}(H_2O)_z + CaCO_3 \quad (7)$$

$$(CaO)_x{\cdot}SiO_2\cdot(H_2O)_y + CO_2 \rightarrow xCaCO_3 + SiO_2{\cdot}(H_2O)_z + (H_2O)_{y\text{-}z} \quad (8)$$

$$3CaO{\cdot}Al_2O_3{\cdot}3CaSO_4{\cdot}32H_2O + 3CO_2 \rightarrow 3CaCO_3 + CaSO_4{\cdot}2H_2O + Al_2O_3{\cdot}xH_2O + (26\text{-}x)\ H_2O \quad (9)$$

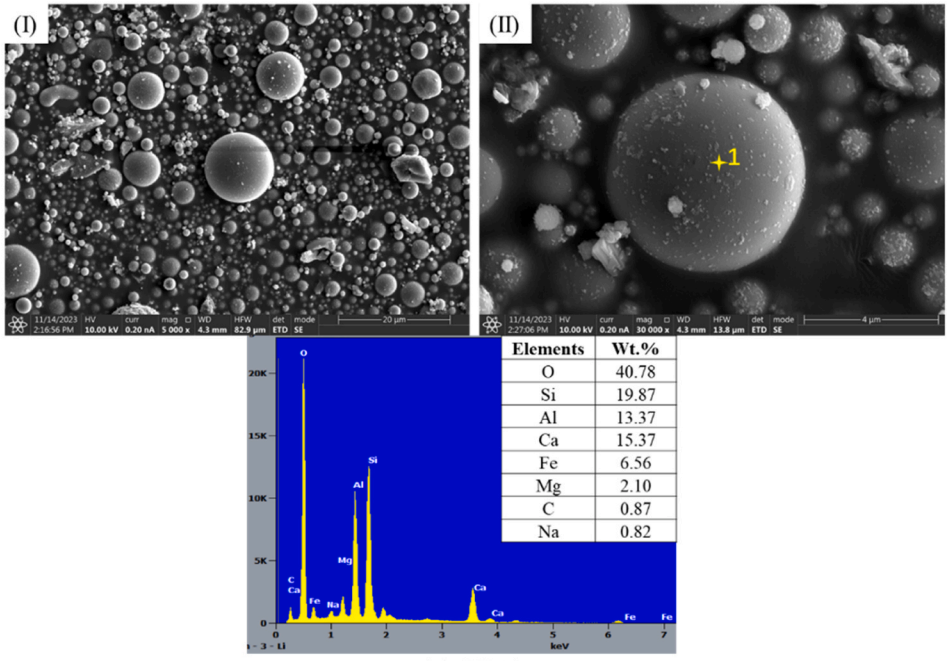

(a) HFA

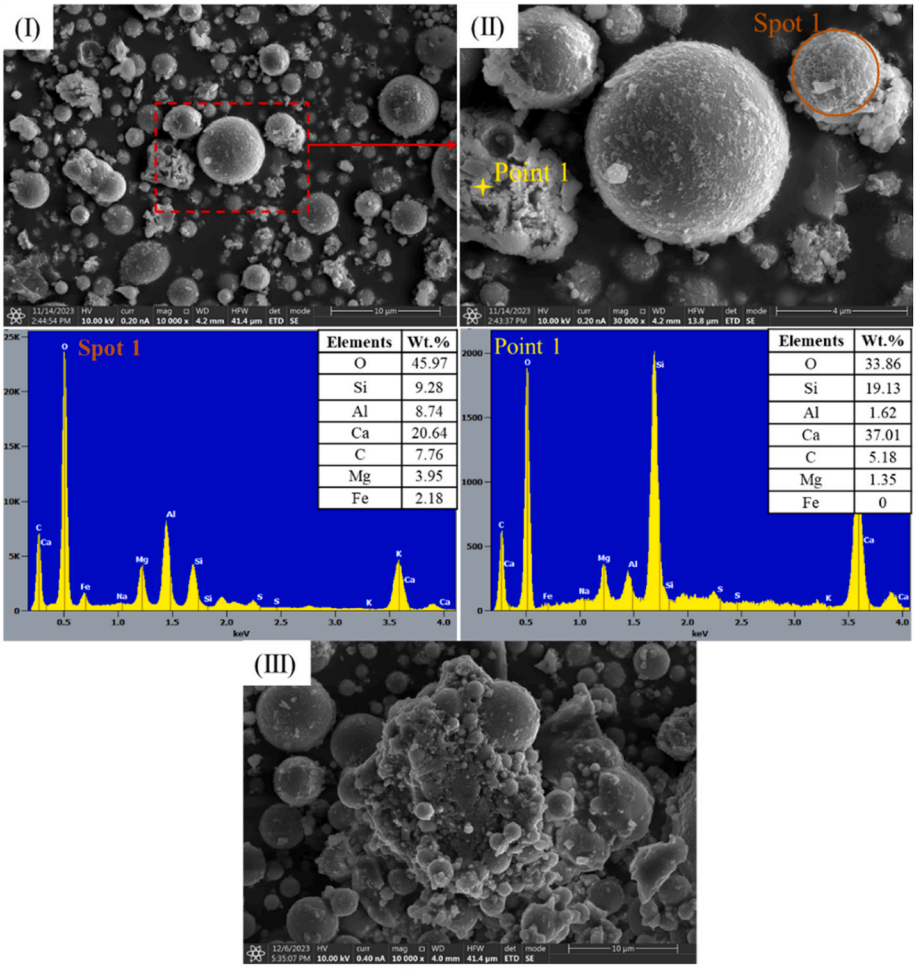

(b) CFA12

Fig. 4. SEM images of HFA before and after carbonation of 12 h.

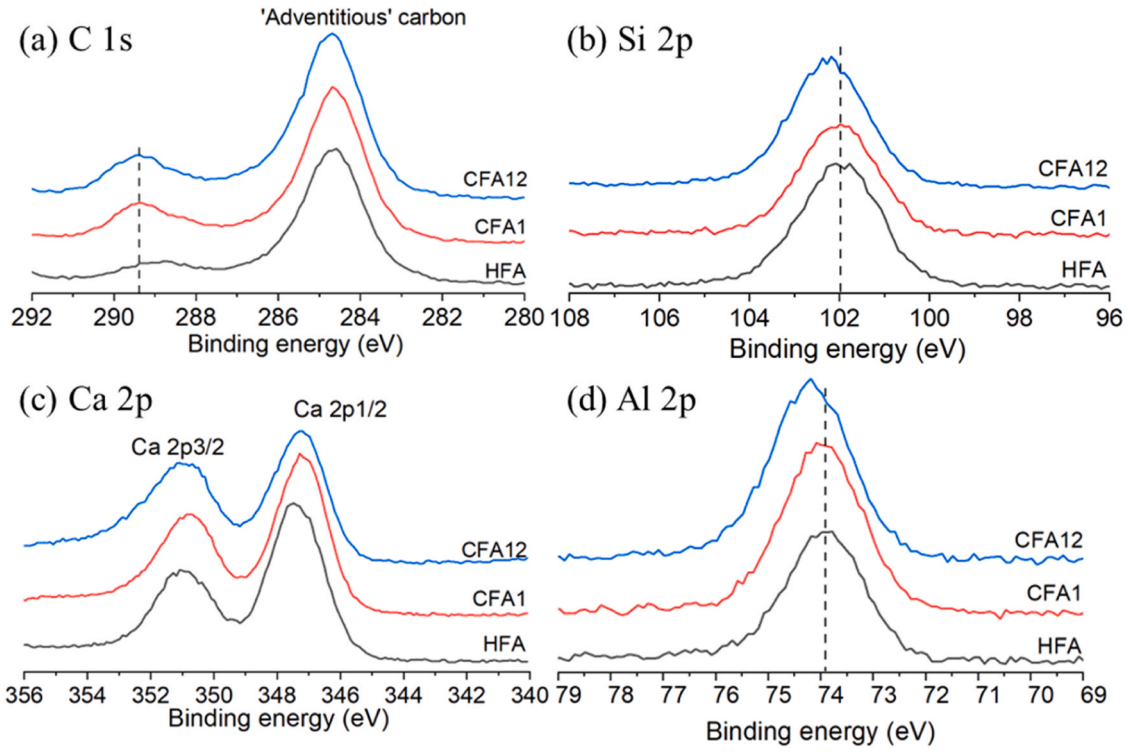

Fig. 5. Photoelectron spectra of HFA and CFA with different carbonation durations.

3.1.2. Effect of carbonation on morphologies of CFA

Fig. 4 shows the morphologies of HFA and CFA12. The original HFA featured spherical particles of different sizes, along with trace amounts of irregular substances on the surface of HFA grains, which should be attributed to hydration or carbonation products in the environment of storage. The EDS identified calcium, silicon, aluminum, iron, magnesium, and traces of C as the main elements in HFA, suggesting possible carbonation on its surface. In contrast, CFA12 exhibited more amorphous products with fibroid and lumpy shapes on the surface of HFA. EDS results (spot 1) implied that these amorphous products precipitated on the surface of HFA were carbonate products. In addition, other products were produced and scattered amid the HFA particles. EDS results (point 1) revealed that the main elements in these products were calcium, silicon, and carbon, indicating a calcium, silicon, and carbon mixed compound. These mixed compounds were likely to be the carbonated products of hatrurite such as calcium carbonate (CC) and silica gels due to the reactions by Eqs. (5–8). It is noteworthy that these mixed products could adhere to the HFA grains (Fig. 4b (II)) and could agglomerate the HFA grains with carbonation products (Fig. 4b (III)), which led to the increased particle size of HFA after carbonation treatment.

3.1.3. Effect of carbonation on surface characteristic of HFA

The surface characteristics of HFA and CFA, carbonated for 1 h and 12 h, were analyzed by XPS, and the results of C 1S, Si 2p, Ca 2p, and Al 2p photoelectron spectra are shown in Fig. 5. The C 1S spectra in Fig. 5 (a) presented two main peaks: the binding energy (BE) of 284.8 eV is attributed to the adventitious carbon due to the sample contamination, and the peak at 289.4 eV is associated with carbonate in $CaCO_3$ [42]. The intensity of the peak linked to CC was observed to increase after the carbonation treatment of HFA due to enhanced CC formation. In Fig. 5 (b), the Si 2p spectra of HFA and CFA indicated no significant changes in intensity, but a slight shift to a higher BE was observed. Previous studies have indicated that the shift of the Si 2p to a higher BE is associated with silicate tetrahedral polymerization [42]. Therefore, the observed shift in the Si 2p peak to a higher BE might be attributed to the formation of highly polymerized silica gel, as supported by the observation in EDS results. The Ca 2p spectra are presented in Fig. 5 (c). No significant changes were noted in the Ca 2p3/2 peak, but the intensity of the Ca 2p1/2 peak decreased slightly. This reduction was attributed to the consumption of hatrurite, typically characterized by a BE around 347 eV [43]. The Al 2p spectra of HFA and CFA are shown in Fig. 5 (d). The Al 2p spectra could be deconvoluted into Al-O and Al-OH components, with the approximate BE of 74 eV and 75 eV, respectively [44,45]. The Al-O was commonly linked to unreacted Al, while Al-OH was associated with reacted Al, typically found in AFm phases and ettringite [44,46]. The Al 2p spectra showed a slight increase in intensity after carbonation treatment of HFA. Given that the XPS analyzed the 5–10 nm surface depth of the samples, the heightened intensity of Al 2p spectra in CFA suggested the dissolution of Al^{3+} during the water mixing and carbonation processes. Furthermore, the spectra displayed a shift towards higher BE with increasing carbonation durations, indicating the formation of aluminate hydrates.

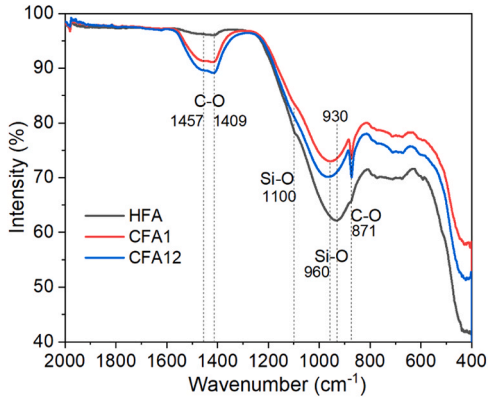

Fig. 6. The FTIR spectra of HFA and CFA with different carbonation durations.

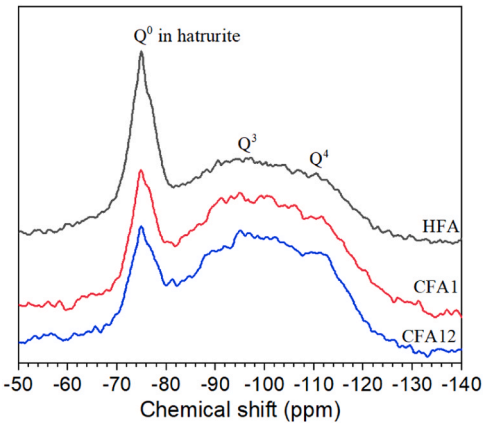

Fig. 7. ^{29}Si NMR spectra of HFA and CFA with different carbonation durations.

3.1.4. *Effect of carbonation on structure development of HFA*

To analyze the structure development of HFA before and after carbonation treatment, FTIR spectra and ^{29}Si and ^{27}Al NMR spectra were collected.

Fig. 6 shows the FTIR spectra of HFA and CFA with different carbonation durations. The bands at around 870 cm^{-1}, 1409 cm^{-1} and 1459 cm^{-1} are attributed to CO_3^{2-} in calcite [47–49]. The FTIR spectrum of HFA presented minor absorptions related to CO_3^{2-}, indicating a small amount of pre-existing $CaCO_3$ in raw material, consistent with the XRD and TG results. After carbonation treatment, a sharp peak at 871 cm^{-1} and two broad peaks at 1409 cm^{-1} and 1459 cm^{-1} were observed in CFA samples due to the calcite formation. It was worth noting that the absorption band at 1459 cm^{-1} could potentially be associated with amorphous $CaCO_3$, as indicated by previous studies [41,50]. This suggested the presence of amorphous $CaCO_3$ formation in CFA, which aligned with the TGA result (Fig. 3 (a)). The bands with wavenumber ranging from 900 cm^{-1} to 1200 cm^{-1} are related to the Si–O asymmetric stretching vibrations [51]. An increase in wavenumber indicated the increased polymerization of silicate [47,52]. It was seen in Fig. 6 that the absorption band at 930 cm^{-1} shifted to a higher wavenumber of 960 cm^{-1}, indicating the formation of highly polymerized Si-rich gel.

The ^{29}Si NMR spectra of HFA and CFA with different carbonation durations are shown in Fig. 7. The ^{29}Si NMR spectra represent the different silicate tetrahedral environments according to the number of connected tetrahedral units to SiO_4^{2-}, and the corresponding assignments for chemical shift have been introduced by previous studies [53–55]. In the spectrum of HFA, a sharp peak at approximately −75 ppm indicated the Q^0 in the hatrurite. Additionally, a broad overlapped peak ranging from −90 to −120 ppm was attributed to Q^3 and Q^4, indicating the presence of highly polymerized silica [56,57]. Carbonation treatment resulted in a decrease of hatrurite while an increase in Q^3 and Q^4 intensity. The increased intensity of Q^3 and Q^4 could be attributed to the formation of Si-rich gels, which confirmed the SEM, XPS and FTIR results. The ^{27}Al NMR spectra of HFA and CFA with different carbonation durations are shown in Fig. 8. Within these spectra, two peaks positioned at −24 ppm and 124 ppm are ascribed to spinning sidebands. The spectrum of HFA exhibited a broad peak centered at 50 ppm, indicative of Al(IV). Following carbonation treatment, the intensity of Al (IV) reduced and a newly formed peak at around 8.5 ppm emerged, indicating Al(VI) likely present in an unknown aluminate product. This aluminate product appears to be an amorphous Al-rich phase, as no characteristic peak assigned to Al-rich products was detected by XRD. A previous study [58] has associated the peak at around 8.5 ppm with amorphous aluminum hydroxide, supporting the interpretation of the observed peak. This verified the XPS results that Al ion was released during the carbonation process under the wet conditions. Through the fitting of the original ^{27}Al NMR spectra, the proportions of Al(IV) and Al (VI) were calculated. The results revealed that there was approximately 21.7 % of Al(VI) in CFA1 and 21.9 % of Al(VI) in CFA12. This indicates that the extension of carbonation duration from 1 h to 12 h did not lead to a significant increase in Al transformation.

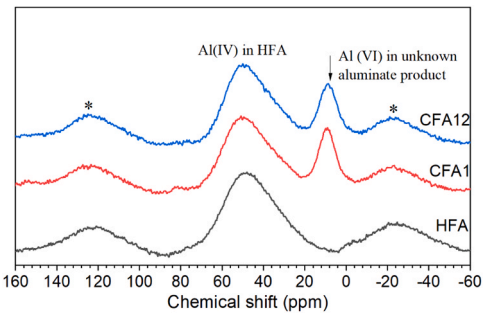

Fig. 8. ^{27}Al NMR spectra of HFA and CFA with different carbonation durations.

To sum up, the accelerated carbonation treatment did not induce substantial structural changes in the HFA. However, it leads to a reduction in the content of hatrurite, a highly reactive component, while generating amorphous CC, Al gel and Si-rich gel.

3.2. *Pozzolanic reactivity test of HFA/CFA-CH blends*

3.2.1. *Heat release of HFA/CFA -CH blends*

Fig. 9 shows the normalized heat release curves by isothermal calorimetry for HFA/CFA-CH blends at 50°C. It is seen in Fig. 9 (a) each sample presented a sharp peak within 1 h, which was attributed to the dissolution of solids within the alkaline solution, as indicated in a prior study [18]. The second peak observed in the calorimetry curves of blends with gypsum (R0G, R1G and R12G) was associated with the formation of C-A-S-H (hydration of hatrurite and pozzolanic reaction of HFA) and ettringite. XRD results (Fig. 10) indicated that, in R0G, R1G and R12G, ettringite formation corresponded with the appearance of the second peak. However, carboaluminate hydrates were scarcely detected in R0G, R1G, and R12G within the timeframe corresponding to the second peak. The absence of carboaluminate hydrates was attributed to the presence of sulfate, which hindered the formation of carboaluminate hydrates [59]. Following the depletion of sulfate, the Mc and Hc were formed; however, Hc ultimately transformed into Mc with the progression of curing age, as Mc was more thermodynamically stable than Hc [60,61]. The second peak was less pronounced in R0, R1, and R12; rather, a broad bump appeared following the first peak. The broad bump was related to the formation of C-A-S-H, Mc and Hc (Fig. 10 (a)). Moreover, the heat flow in R0 was higher than R1 between 1 and 5 hours, suggesting that during this initial period (before 5 h), carbonation hindered the pozzolanic reactivity of HFA. It is interesting to note that gypsum seemed to retard the pozzolanic reactivity of both HFA and CFA compared to the blends without gypsum, resulting in an “induction period” before the appearance of the second peak. This retardation effect reduced the heat release within 8 h compared with the blends without gypsum, as shown in Fig. 9 (b).

The cumulative heat release curves for HFA/CFA-CH blends at 50°C are shown in Fig. 9 (b). The cumulative heat release curves exhibited a rapid ascent within the initial 25 h, followed by a gradual increase, with the rate of increase decreasing over time. The impact of carbonation treatment on the pozzolanic reaction heat of HFA differed in HFA/CFA-CH systems with and without gypsum. In systems without gypsum, accelerated carbonation treatment did not significantly affect the heat release of HFA. However, in the presence of gypsum, carbonation treatment reduced the pozzolanic reaction heat, and this reduction primarily resulted from the initial 20 h, involving the dissolution of raw materials and formation of ettringite and C-(A-)S-H. Additionally, sulfate accelerated the pozzolanic reaction of HFA, comparing R0G with R0. However, this acceleration effect was diminished with increasing

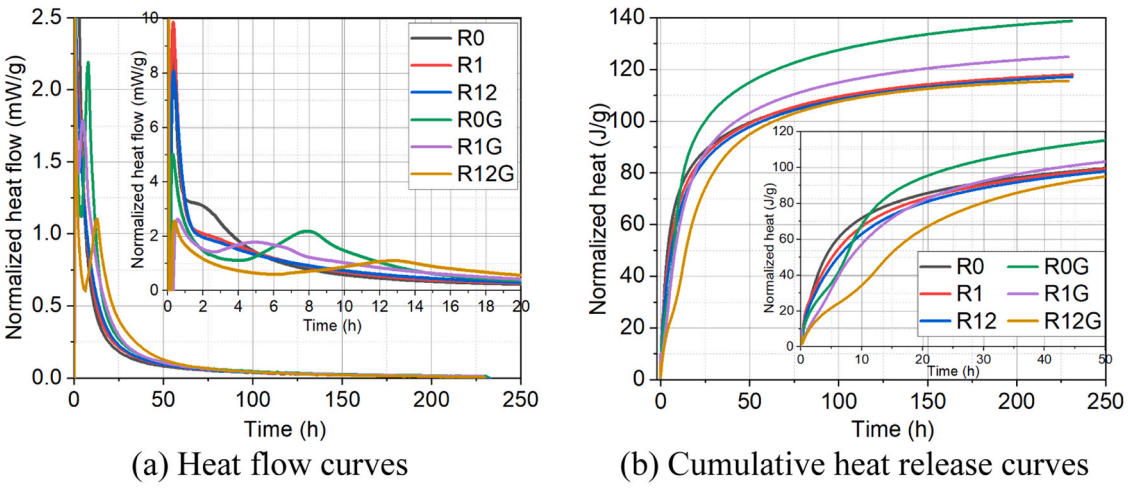

Fig. 9. Heat release for HFA/CFA-CH blends at 50°C.

carbonation durations, to the extent that even for R12G, sulfate did not seem favorable to the pozzolanic reactivity of CFA.

Fig. 11 shows the normalized heat release curves by isothermal calorimetry for HFA/CFA-CH blends without gypsum at 20°C. The corresponding XRD results at 10d are shown in Fig. 12. The heat flow evolution of blends at 20°C also exhibited a broad bump resembling that of blends at 50°C, albeit appearing later. This delay was attributed to the slower pozzolanic reaction at lower temperatures, contrasting with the accelerated reaction observed at 50°C. The cumulative heat release results indicated that the carbonation treatment reduced the pozzolanic reactivity of HFA when tested at 20°C, contrary to the observation in Fig. 9 (b) that carbonation treatment did not significantly affect the heat release of HFA in the systems at 50°C without gypsum. Moreover, comparing the cumulative heat release at 50°C and 20°C revealed that elevated temperatures led to an around 10 J/g increase in cumulative heat of HFA. For CFA1 and CFA12, elevated temperatures resulted in a more substantial rise in the cumulative heat, increasing by 20 and 34 J/g, respectively. This suggested that elevated temperatures had a more pronounced effect on promoting the pozzolanic reaction of CFA. The possible reasons are explained as follows. Carbonation treatment led to a decrease in the proportions of highly reactive components, including hatrurite and certain amorphous phases, while resulting in the production of calcite – a less reactive phase. Consequently, in the CFA-CH blends at 20°C, the cumulative heat release of CFA was reduced due to the reduction of highly reactive components. Although the formation of Mc – from the less reactive calcite – could compensate for the reaction heat, this compensation might have been insufficient. As presented in Fig. 12, a distinct peak for calcite was observed. However, at 50°C, more Mc was produced, consuming a significant portion of the calcite, as illustrated in Fig. 13 (a). This increased formation of Mc at higher temperatures could potentially compensate for the reduced cumulative heat release.

3.2.2. *Phase assemblage analysis*

Fig. 13 shows the XRD patterns and QXRD results of HFA/CFA-CH cured at 50°C for 10d. Due to the poor crystalline structure of C-(A-)S-H, it was considered amorphous during the QXRD analysis. Therefore, the amorphous phases in Fig. 13 (b) should consist of C-(A)-S-H, amorphous components in unreacted HFA, and other possible amorphous products. In the case of gypsum-free blends, Mc (main peak at 11.7° 2θ) and amorphous phases, including C-(A-)S-H, constituted the main reaction products. A minor quantity of Mc was formed in R0, whereas the contents of Mc in R1 and R12 are notably higher, attributed to the increased availability of calcite.

Compared to blends without gypsum, less calcite was consumed in blends with gypsum, leading to less formation of Mc. The reduced formation of Mc was attributed to a competition effect between sulfate and carbonate for Al_2O_3, with the presence of gypsum favoring the formation

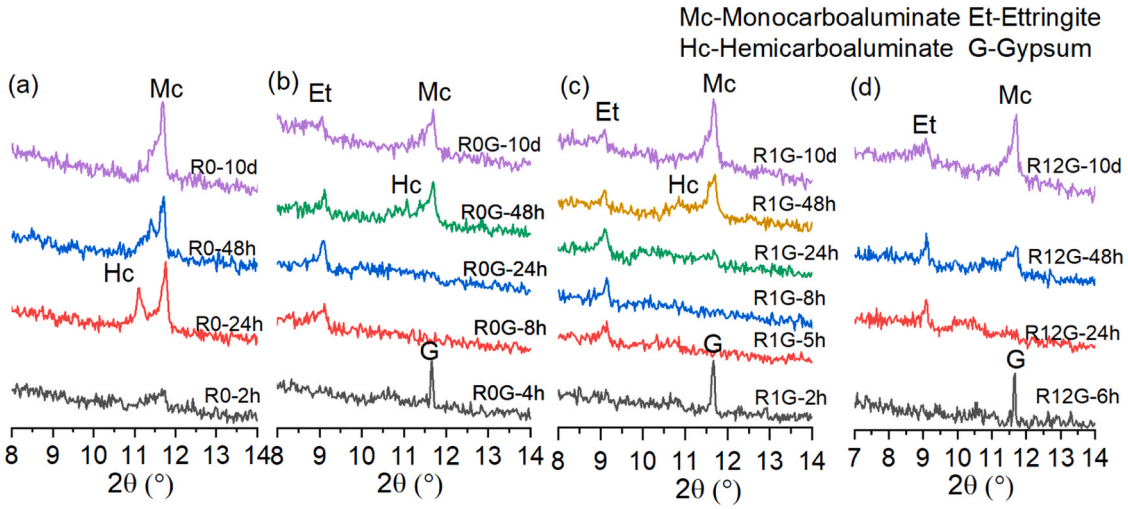

Fig. 10. XRD patterns of HFA/CFA-CH blends at different ages of hydration.

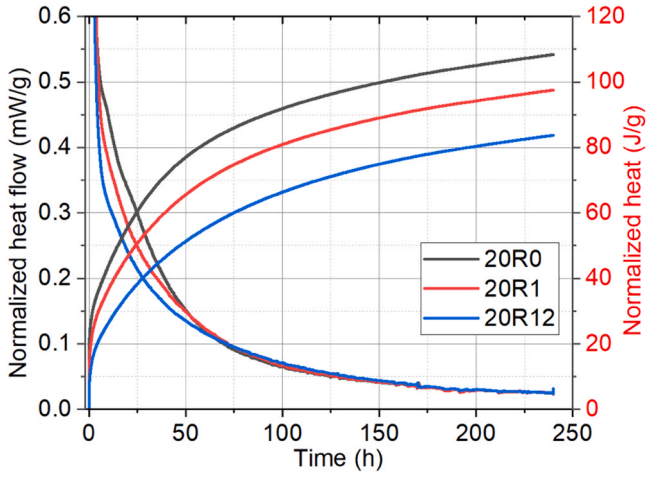

Fig. 11. Heat release for HFA/CFA-CH blends at 20°C.

of ettringite while restricting the formation of Mc. Moreover, the potential of ettringite formation in R1G and R12G appeared to be reduced by the carbonation treatment as compared to R0G, likely due to the dilution of the Al content in CFA caused by the formation of CC.

3.2.3. *Ions evolution in HFA/CFA-CH slurries*

To investigate the ions evolution during the pozzolanic reaction of HFA and CFA, a slurry of HFA/CFA-CH was prepared. Fig. 14 shows the concentration evolution of Al, Si, and S ions in HFA/CFA-CH at intervals of 1d, 3d, and 10d, and the corresponding results are given in Table 2. In the case of gypsum-free slurry, the concentration of Si and S did not show noticeable changes over reaction time. Additionally, the impact of carbonation treatment on the dissolution of Si and S ions was negligible. It is worth noting that the S detected in gypsum-free slurry originated from raw HFA. For Al, the highest concentration was observed in R0–1d, and with time increasing, the concentration of Al decreased due to the formation of Mc and Hc (mainly Mc). However, the concentration of Al in R1 and R12 was lower compared to R0 across all reaction time durations, and the concentration of Al in R1 and R12 only decreased slightly over reaction time. This was attributed to the availability of CC in R0 and R12, which accelerated the formation of Mc, reducing Al levels rapidly within a short time (1d). Similarly, in gypsum-containing slurries, the concentration of Al was slightly higher in R0G compared to R1G and R12G due to a greater consumption of Al through reactions with CC. The concentration of S was high in gypsum-containing slurries, with R12G exhibiting the highest concentration, followed by R1 and then R0. This difference could be due to the competition effect between

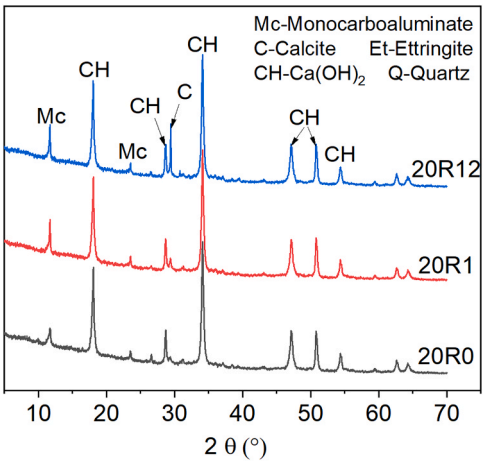

Fig. 12. XRD patterns of HFA/CFA-CH blends cured at 20°C for 10d.

sulfate and carbonate for Al, which limited the formation of ettringite. Besides, the dilution of the content of Al in CFA by the formation of CC also decreased the formation of ettringite, as shown in Fig. 13 (b), which leads to less sulfate consumption in R12G.

4. Discussion

The pozzolanic reactivity of SCMs is generally influenced by a combination of physical and chemical factors. Physical factors encompass particle size distribution, surface morphology, specific surface area, and curing conditions, while chemical factors involve mineral composition, microstructural properties, solution composition, etc. [19]. When the extrinsic aspects remain the same in a pozzolanic reactivity test of SCMs, the SCMs with more reactive components, such as glassy or amorphous phases, higher surface area, and smaller particle size, are expected to exhibit high pozzolanic reactivity.

In the context of this study, from the chemical aspects, accelerated carbonation treatment of HFA led to a decrease in highly reactive components such as hatrurite and certain amorphous phases, resulting in the formation of calcite (a less reactive phase) and other amorphous phases such as ACC, Al gel, and Si gel, which conversely diluted the highly reactive components. However, no obvious changes in the chemical structure of fly ash (due to the carbonation treatment) were observed in FTIR and NMR results. Regarding physical aspects, the particle size of the fly ash increased after carbonation treatment, but at the same time the surface area also increased. As shown in Fig. 15, the BET specific surface area increased with carbonation durations. This could be due to the formation of amorphous nano-scale-sized particles on the surface of raw material grains (Fig. 4). It is noted that the change in specific surface area observed in this study contrasts with findings from a previous study [13], where carbonation treatment of HFA reduced the specific surface area. The differences could be attributed to variations in HFA compositions, particle size distribution, and carbonation treatment conditions, such as CO_2 concentration and carbonation duration, etc. This implies that carbonation treatment parameters may affect the properties of CFA and thus its pozzolanic reactivity, which should be further investigated in future studies.

The composition of HFA primarily consists of around 80 % of amorphous phase, around 10 % of hatrurite, a small amount of calcite (1.4 %), and the remaining less than 9 % of quartz and brownmillerite. Considering the reaction heat of quartz and brownmillerite is negligible, the reaction of amorphous phases, hatrurite and calcite contributes to the cumulative heat in the HFA-CH blends. In the case of CFA-CH blends, although the highly reactive components were diminished due to the carbonation reaction and dilution effect by the resulting products, the newly formed CC, notably ACC, along with amorphous Al gel and Si gel could accelerate the formation of Mc (main) and C-(A-)S-H, compensating for the reduced heat. Additionally, as the dissolution of SCMs increased with increasing surface area [19], the increased surface area was also favorable for the pozzolanic reaction of CFA. Hence, in the HFA/CFA-CH tests, the carbonation-treated fly ash exhibited a comparable pozzolanic reactivity to that of HFA, while permanently storing CO_2.

Yet, within the HFA/CFA-CH blends incorporating gypsum, the carbonation treatment had negative effects on the pozzolanic reactivity. The reaction of CC and Al starts only after the depletion of gypsum. Within 24 h, the gypsum facilitated the formation of low-solubility ettringite and consumed most of Al, as illustrated in Table 2. Consequently, the availability of Al was limited, resulting in a reduction in Mc formation. This decrease in Mc formation correlated with diminished heat release, which otherwise would have compensated for the reduced heat owing to the decline in active components and the dilution effect.

The above findings indicate that the quantity of reacted CC is constrained by the availability of Al, implying the importance of Al in studying the pozzolanic reactivity of carbonated SCMs through isothermal calorimetry method. Moreover, since the reaction between

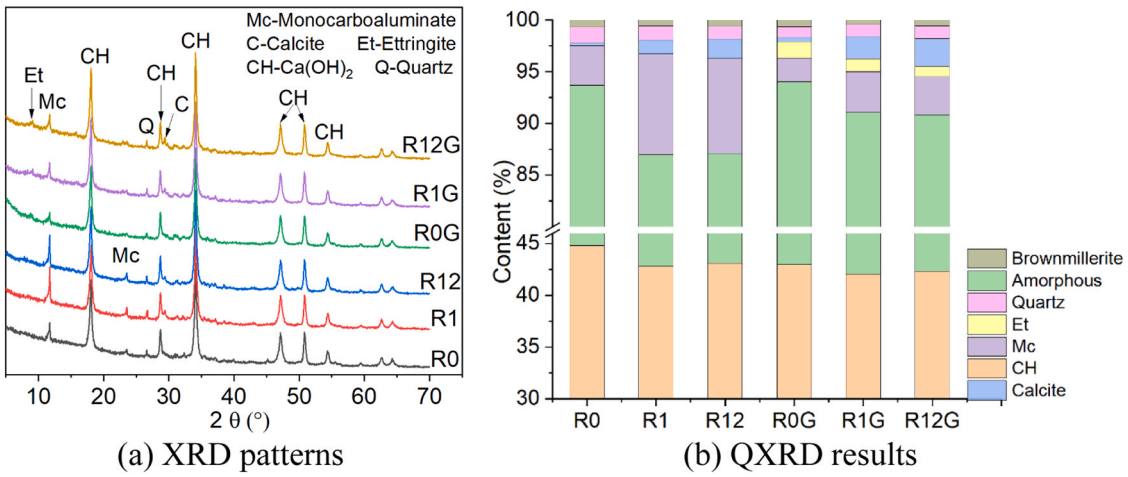

Fig. 13. XRD results of HFA/CFA-CH blends at 10d.

CC and Al begins only upon the depletion of gypsum [61], the contribution of CC to the reaction heat through the formation of Mc and Hc can be diminished in the presence of gypsum. This suggests that when assessing the pozzolanic reactivity of carbonated SCMs, it's crucial to thoroughly account for the SCMs' reaction conditions, such as solution compositions.

5. Conclusion

This study investigated the impact of carbonation treatment on the physical and chemical properties of high-calcium fly ash (HFA), aiming to understand how carbonation influences its pozzolanic reactivity, and then evaluated the pozzolanic reactivity of carbonated HFA (CFA) by monitoring the heat release of HFA/CFA-CH blends. Based on the experimental results, several conclusions are drawn as follows.

(1) The accelerated carbonation treatment alters the physical properties of HFA, including particle size, surface characteristics, morphology and phase assemblage, but barely influences the chemical structure.

(2) In HFA/CFA-CH blends, carbonation treatment has a marginal influence on the pozzolanic reactivity of the fly ash. Although the highly reactive components can be reduced due to the carbonation pretreatment and the dilution effect by the reaction products, the newly formed CC, especially ACC, and amorphous Al gel and Si gel can accelerate the formation of Mc (main) and C-(A-)S-H, compensating for the reduced heat resulting from the diminished highly reactive

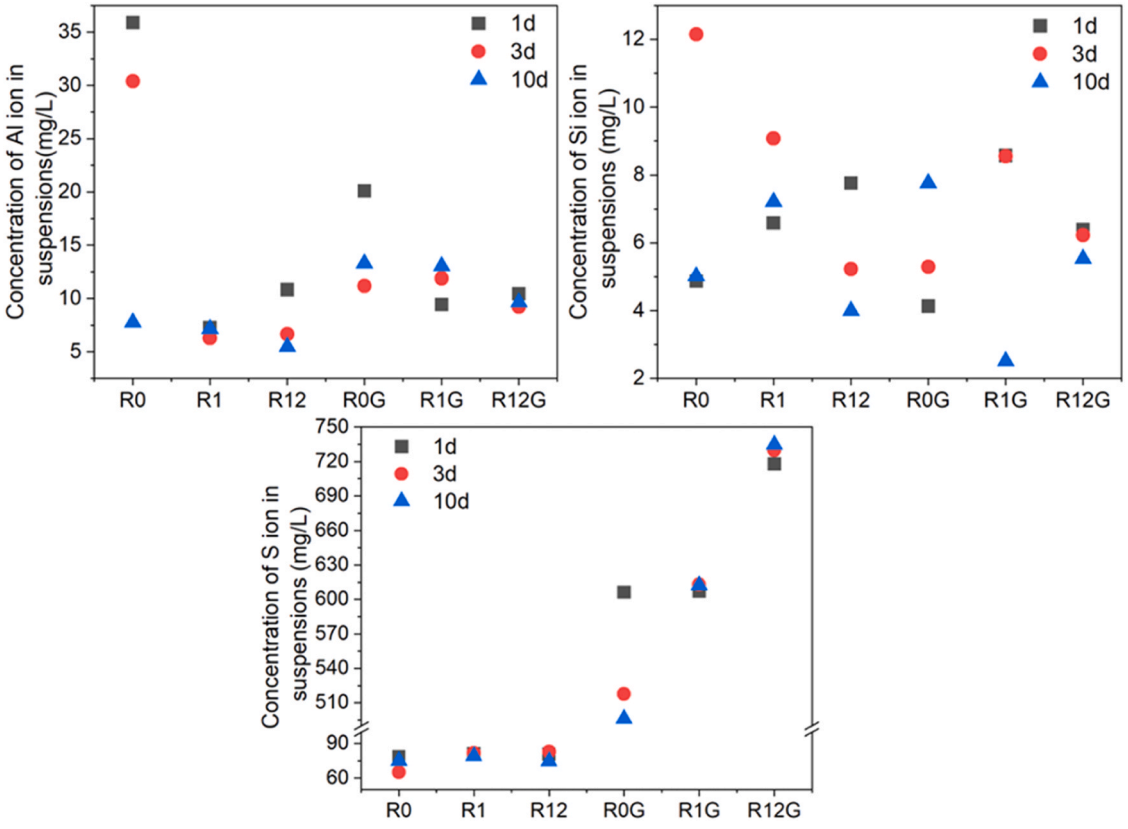

Fig. 14. The concentration of Al, Si, and S ions in suspensions (mg/L) determined by ICP-OES.

Table 2
The concentration of dissolved ions in suspensions (mg/L) determined by ICP-OES.

Samples	Al	Si	S	Samples	Al	Si	S
R0–1d	35.88	4.87	78.73	R0G−1d	20.08	4.13	606.14
R0–3d	30.38	12.15	65.09	R0G−3d	11.19	5.29	517.73
R0–10d	7.75	5.01	74.79	R0G−10d	13.28	7.75	496.02
R1–1d	7.26	6.58	81.23	R1G−1d	9.42	8.57	606.88
R1–3d	6.29	9.07	81.84	R1G−3d	11.88	8.55	612.96
R1–10d	7.13	7.20	79.06	R1G−10d	13.04	2.51	612.17
R12–1d	10.82	7.76	80.92	R12G−1d	10.45	6.38	717.95
R12–3d	6.66	5.22	82.64	R12G−3d	9.21	6.22	729.91
R12–3d	5.47	3.99	74.66	R12G−10d	9.63	5.53	734.74

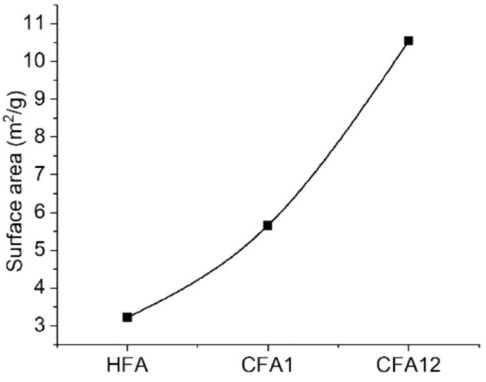

Fig. 15. Specific surface area of HFA and CFA with different carbonation durations determined by BET.

components. Additionally, the increased surface area is favorable for the pozzolanic reaction of CFA. Furthermore, the carbonation reactivity of CFA appears to depend on the curing temperature, with a high temperature of 50°C accelerating its pozzolanic reaction.

(3) In the HFA/CFA-CH blends containing gypsum, carbonation treatment adversely affects the pozzolanic reactivity of fly ash. Gypsum facilitates the formation of low-solubility ettringite, which consumes most of the Al within 24 h. This process limits the availability of Al, thereby reducing the formation of Mc and resulting in a decrease in heat release.

(4) The degree to which CC can be reacted is constrained by the availability of Al, which implies the importance of Al in determining the pozzolanic reactivity of carbonated HFA as characterized by isothermal calorimetry.

To sum up, upon being proportioned and used properly, the carbonation-treated fly ash can retain comparable pozzolanic reactivity to that of the untreated ash while storing CO_2 permanently in the supplementary cementitious material and in concrete. However, the HFA used in this research may not represent common high-calcium fly ashes due to the absence of free lime and the presence of hatrurite. Further verification may be needed to confirm if the conclusions are commonly valid.

CRediT authorship contribution statement

Hongyan Ma: Writing – review & editing, Supervision, Resources, Funding acquisition, Conceptualization. **Yongjia he:** Writing – review & editing, Supervision, Conceptualization. **Linnu Lu:** Writing – review & editing. **Gao Deng:** Writing – original draft, Validation, Methodology, Investigation, Formal analysis, Data curation, Conceptualization. **Nannan Zhang:** Writing – original draft, Validation, Methodology, Investigation, Formal analysis, Data curation. **Wenyu Liao:** Writing – review & editing. **Lingyu Chi:** Methodology.

Declaration of Competing Interest

The authors declare that they have no known competing financial interests or personal relationships that could have appeared to influence the work reported in this paper.

Data availability

Data will be made available on request.

Acknowledgements

This material is based upon work supported by the National Science Foundation under Grant No. 2219086. Any opinions, findings, and conclusions or recommendations expressed in this material are those of the author(s) and do not necessarily reflect the views of the National Science Foundation.

References

[1] https://www.ecocemglobal.com/en-us/our-company/the-future-of-cement.
[2] G. Habert, S.A. Miller, V.M. John, J.L. Provis, A. Favier, A. Horvath, K.L. Scrivener, Environmental impacts and decarbonization strategies in the cement and concrete industries, Nat. Rev. Earth Environ. (2020).
[3] P. Shen, Y. Jiang, Y. Zhang, S. Liu, D. Xuan, J. Lu, S. Zhang, C.S. Poon, Production of aragonite whiskers by carbonation of fine recycled concrete wastes: an alternative pathway for efficient CO2 sequestration, Renew. Sustain. Energy Rev. (2023) 173.
[4] J. Wei, C. Fang, B. Zhou, Z. Wu, Effect of organic phosphonate types on performance of alkali-activated slag-based materials and its mechanism, Cem. Concr. Compos. 151 (2024).
[5] G. Deng, He Yongjia, Lu Linnu, Wang Fazhou, Hu Shuguang, Comparison between fly ash and slag slurry in various alkaline environments: dissolution, migration, and coordination state of aluminum, ACS Sustain. Chem. Eng. 9 (2021) 12109–12119.
[6] Q.Q. Biqin Dong, Zhentao Gu, Jiaqi Xiang, Canjie Huang, Yuan Fang, Feng Xing, Wei Liu, Characterization of carbonation behavior of fly ash blended cement materials by the electrochemical impedance spectroscopy method, Cem. Concr. Compos. 65 (2016) 118–127.
[7] G. Deng, Y. He, L. Lu, S. Hu, Evolution of aluminate hydrate phases in fly ash-cement system under the sulfate conditions, Constr. Build. Mater. (2020) 252.
[8] C. Siriruang, P. Toochinda, P. Julnipitawong, S. Tangtermsirikul, CO2 capture using fly ash from coal fired power plant and applications of CO2-captured fly ash as a mineral admixture for concrete, J. Environ. Manag. 170 (2016) 70–78.
[9] D. Wang, C. Xiong, W. Li, J. Chang, Growth of calcium carbonate induced by accelerated carbonation of tricalcium silicate, ACS Sustain. Chem. Eng. 8 (39) (2020) 14718–14731.
[10] P. Chen, J. Wang, L. Wang, Y. Xu, X. Qian, H. Ma, Producing vaterite by CO2 sequestration in the waste solution of chemical treatment of recycled concrete aggregates, J. Clean. Prod. 149 (2017) 735–742.
[11] C.S. Poon, P. Shen, Y. Jiang, Z. Ma, D. Xuan, Total recycling of concrete waste using accelerated carbonation: a review, Cem. Concr. Res. 173 (2023).
[12] M. Zajac, I. Maruyama, A. Iizuka, J. Skibsted, Enforced carbonation of cementitious materials, Cem. Concr. Res. 174 (2023).
[13] T. Chen, M. Bai, X. Gao, Carbonation curing of cement mortars incorporating carbonated fly ash for performance improvement and CO2 sequestration, J. CO2 Util. (2021) 51.
[14] S.-L. Pei, S.-Y. Pan, X. Gao, Y.-K. Fang, P.-C. Chiang, Efficacy of carbonated petroleum coke fly ash as supplementary cementitious materials in cement mortars, J. Clean. Prod. 180 (2018) 689–697.
[15] A. Su, T. Chen, X. Gao, Q. Li, L. Qin, Effect of carbonation curing on durability of cement mortar incorporating carbonated fly ash subjected to Freeze-Thaw and sulfate attack, Constr. Build. Mater. (2022) 341.
[16] I. Mehdipour, K.H. Khayat, Effect of particle-size distribution and specific surface area of different binder systems on packing density and flow characteristics of cement paste, Cem. Concr. Compos. 78 (2017) 120–131.
[17] Y. Liu, Q. Yuan, Y. Tan, M.J. Garba, Comparative analysis and modification of evaluation methods for the pozzolanic reactivity of natural volcanic powders, J. Build. Eng. 78 (2023).
[18] J. Yoon, K. Jafari, R. Tokpatayeva, S. Peethamparan, J. Olek, F. Rajabipour, Characterization and quantification of the pozzolanic reactivity of natural and non-conventional pozzolans, Cem. Concr. Compos. (2022) 133.
[19] J. Skibsted, R. Snellings, Reactivity of supplementary cementitious materials (SCMs) in cement blends, Cem. Concr. Res. (2019) 124.
[20] T. Hemalatha, A. Ramaswamy, A review on fly ash characteristics – towards promoting high volume utilization in developing sustainable concrete, J. Clean. Prod. 147 (2017) 546–559.
[21] Z. Li, G. Xu, X. Shi, Reactivity of coal fly ash used in cementitious binder systems: a state-of-the-art overview, Fuel 301 (2021).
[22] P.P. Sivakumar, S. Matthys, N. De Belie, E. Gruyaert, Reactivity assessment of modified ferro silicate slag by R3 method, Appl. Sci. 11 (1) (2021).

[23] H. Wang, X. Liu, Z. Zhang, Pozzolanic activity evaluation methods of solid waste: a review, J. Clean. Prod. 402 (2023).
[24] T. Matschei, B. Lothenbach, F.P. Glasser, The role of calcium carbonate in cement hydration, Cem. Concr. Res. 37 (4) (2007) 551–558.
[25] B. Lothenbach, M. Zajac, Application of thermodynamic modelling to hydrated cements, Cem. Concr. Res. 123 (2019).
[26] B. Lothenbach, G. Le Saout, E. Gallucci, K. Scrivener, Influence of limestone on the hydration of Portland cements, Cem. Concr. Res. 38 (6) (2008) 848–860.
[27] C. Hu, Y. Ruan, S. Yao, F. Wang, Y. He, Y. Gao, Insight into the evolution of the elastic properties of calcium-silicate-hydrate (C-S-H) gel, Cem. Concr. Compos. (2019) 104.
[28] D. Hou, C. Wu, Q. Yang, W. Zhang, Z. Lu, P. Wang, J. Li, Q. Ding, Insights on the molecular structure evolution for tricalcium silicate and slag composite: from 29Si and 27Al NMR to molecular dynamics, Compos. Part B Eng. (2020) 202.
[29] F. Avet, R. Snellings, A. Alujas Diaz, M. Ben Haha, K. Scrivener, Development of a new rapid, relevant and reliable (R3) test method to evaluate the pozzolanic reactivity of calcined kaolinitic clays, Cem. Concr. Res. 85 (2016) 1–11.
[30] S. Donatello, M. Tyrer, C.R. Cheeseman, Comparison of test methods to assess pozzolanic activity, Cem. Concr. Compos. 32 (2) (2010) 121–127.
[31] M. Kasaniya, M.D.A. Thomas, E.G. Moffatt, Pozzolanic reactivity of natural pozzolans, ground glasses and coal bottom ashes and implication of their incorporation on the chloride permeability of concrete, Cem. Concr. Res. 139 (2021).
[32] P. Suraneni, J. Weiss, Examining the pozzolanicity of supplementary cementitious materials using isothermal calorimetry and thermogravimetric analysis, Cem. Concr. Compos. 83 (2017) 273–278.
[33] P. Suraneni, T. Fu, V. Jafari Azad, O.B. Isgor, J. Weiss, Pozzolanicity of finely ground lightweight aggregates, Cem. Concr. Compos. 88 (2018) 115–120.
[34] D. Wang, J. Chang, W.S. Ansari, The effects of carbonation and hydration on the mineralogy and microstructure of basic oxygen furnace slag products, J. CO2 Util. 34 (2019) 87–98.
[35] Y. Wang, Z. Shui, X. Gao, Y. Huang, R. Yu, Q. Song, Chloride binding capacity and phase modification of alumina compound blended cement paste under chloride attack, Cem. Concr. Compos. (2020) 108.
[36] Y.-R. Yi, Y. Lin, Y.-C. Du, S.-q Bai, Z.-l Ma, Y.-g Chen, , Accelerated carbonation of ladle furnace slag and characterization of its mineral phase, Constr. Build. Mater. (2021) 276.
[37] N. Saeki, L. Cheng, R. Kurihara, T. Ohkubo, A. Teramoto, Y. Suda, R. Kitagaki, I. Maruyama, Natural carbonation process in cement paste particles in different relative humidities, Cem. Concr. Compos. (2023).
[38] D. Zhang, Z. Ghouleh, Y. Shao, Review on carbonation curing of cement-based materials, J. CO2 Util. 21 (2017) 119–131.
[39] D. Zhang, V.C. Li, B.R. Ellis, Ettringite-related dimensional stability of CO2-cured portland cement mortars, ACS Sustain. Chem. Eng. 7 (19) (2019) 16310–16319.
[40] Y. Mu, Z. Liu, F. Wang, Comparative study on the carbonation-activated calcium silicates as sustainable binders: reactivity, mechanical performance, and microstructure, ACS Sustain. Chem. Eng. 7 (7) (2019) 7058–7070.
[41] P. Shen, Y. Zhang, Y. Jiang, B. Zhan, J. Lu, S. Zhang, D. Xuan, C.S. Poon, Phase assemblance evolution during wet carbonation of recycled concrete fines, Cem. Concr. Res. 154 (2022).
[42] L. Black, K. Garbev, I. Gee, Surface carbonation of synthetic C-S-H samples: a comparison between fresh and aged C-S-H using X-ray photoelectron spectroscopy, Cem. Concr. Res. 38 (6) (2008) 745–750.
[43] L. Black, A. Stumm, K. Garbev, P. Stemmermann, K.R. Hallam, G.C. Allen, X-ray photoelectron spectroscopy of the cement clinker phases tricalcium silicate and β-dicalcium silicate, Cem. Concr. Res. 33 (10) (2003) 1561–1565.
[44] X. Wang, W. Ni, X. Wei, S. Zhang, J. Li, W. Hu, Promotion effects of gypsum on carbonation of aluminates in medium Al ladle furnace refining slag, Constr. Build. Mater. (2022) 336.
[45] H. Abedini Najafabadi, N. Ozalp, M. Epstein, R. Davis, Solar carbothermic reduction of dolime as a promising option to produce magnesium and calcium, Ind. Eng. Chem. Res. 58 (51) (2019) 23540–23548.
[46] R.N.J. Comans, T.T. Eighmy, E.L. Shaw, Reference spectra for environmentally important secondary minerals: ettringite (Ca6Al2(SO4)3(OH)12·26H2O) by XPS, Surf. Sci. Spectra 4 (2) (1996) 150–156.
[47] Y. Zhao, X. Hu, Q. Yuan, C. Shi, The change of phase assemblage and desorption of bound chloride for seawater cement paste under sulfate attack, Cem. Concr. Compos. 139 (2023).
[48] A. Ćwik, I. Casanova, K. Rausis, K. Zarębska, Utilization of high-calcium fly ashes through mineral carbonation: the cases for Greece, Poland and Spain, J. CO2 Util. 32 (2019) 155–162.
[49] L. Regev, K.M. Poduska, L. Addadi, S. Weiner, E. Boaretto, Distinguishing between calcites formed by different mechanisms using infrared spectrometry: archaeological applications, J. Archaeol. Sci. 37 (12) (2010) 3022–3029.
[50] C. Günther, A. Becker, G. Wolf, M. Epple, In vitro synthesis and structural characterization of amorphous calcium carbonate, zeitschrift für, Anorg. Allg. Chem. 631 (13-14) (2005) 2830–2835.
[51] I. García Lodeiro, D.E. Macphee, A. Palomo, A. Fernández-Jiménez, Effect of alkalis on fresh C–S–H gels. FTIR analysis, Cem. Concr. Res. 39 (3) (2009) 147–153.
[52] I.F. Sáez del Bosque, S. Martínez-Ramírez, M.T. Blanco-Varela, FTIR study of the effect of temperature and nanosilica on the nano structure of C–S–H gel formed by hydrating tricalcium silicate, Constr. Build. Mater. 52 (2014) 314–323.
[53] X. Pardal, F. Brunet, T. Charpentier, I. Pochard, A. Nonat, 27Al and 29Si solid-state NMR characterization of calcium-aluminosilicate-hydrate, Inorg. Chem. 51 (3) (2012) 1827–1836.
[54] G. Deng, Y. He, L. Lu, S. Hu, The effect of activators on the dissolution characteristics and occurrence state of aluminum of alkali-activated metakaolin, Constr. Build. Mater. (2020) 235.
[55] P. Ma, W. Liao, Y. Zhuo, H. Ma, Y. Zhu, G. Chen, Characterization of alkali-silica reaction (ASR) products and C-S-H using SWIR spectroscopy for nondestructive detection of ASR, Constr. Build. Mater. (2024) 416.
[56] I. Elkhadiri, F. Puertas, The effect of curing temperature on sulphate-resistant cement hydration and strength, Constr. Build. Mater. 22 (7) (2008) 1331–1341.
[57] S.A.Á. Palomo, A. Fernandez-Jiménez, I. Sobrados, J. Sanz, Alkaline activation of fly ashes NMR study of the reaction products, J. Am. Ceram. Soc. 87 (2004) 1141–1145.
[58] T.W.T. Isobe, J.B. d'Espinose de la Caillerie, A.P. Legrand, D. Massiot Solid-state 1H and 27Al NMR studies of amorphous aluminum hydroxides, J. Colloid Interface Sci. 261 (2003) 320–324.
[59] H. Huang, X. Li, F. Avet, W. Hanpongpun, K. Scrivener, Strength-promoting mechanism of alkanolamines on limestone-calcined clay cement and the role of sulfate, Cem. Concr. Res. 147 (2021).
[60] C. Li, S. Krishnya, M. Ogino, E. Owaki, Y. Elakneswaran, Investigating the hydration characteristics of a new composite cementitious binder containing of slag and calcite, Constr. Build. Mater. 361 (2022).
[61] M. Zajac, A. Rossberg, G. Le Saout, B. Lothenbach, Influence of limestone and anhydrite on the hydration of Portland cements, Cem. Concr. Compos. 46 (2014) 99–108.